3D Imaging with CMOS Single-Photon Detector Arrays for Space Applications: Ground-Based Measurements and Irradiation Tests

Matteo Perenzoni[1], Daniele Perenzoni[1], David Stoppa[1], Alexandre Pollini[2], Jacques Haesler[2], Christophe Pache[2]
[1]*Fondazione Bruno Kessler, Trento, Italy*
[2]*CSEM, Neuchatel, Switzerland*

Introduction. An increasing and heterogeneous number of applications is requiring precise awareness of the environment through image sensors, spanning from autonomous driving to gaming or industrial control. In many of these applications, and in particular in the field of space navigation, rendez-vous and landing with high relative velocity instrument-target, the requirements in terms of robustness and frame rate make the objective quite challenging. One of the imaging techniques which can be chosen as a solution is direct time-of-flight (DTOF), and an interesting technology able to respond to the implementation needs is represented by CMOS single-photon avalanche diodes (SPAD), with specialized processing circuitry enabling the integration of smart features. With this configuration, a light pulse is emitted to the scene, and its back-reflected echo is detected by the single-photon device, while the CMOS circuit implements the "stopwatch" function needed to measure the time-of-flight. In this paper, the sensor realized in [1] is employed in a light detection and ranging (LiDAR) system able to realize both 3D imaging and single-point distance measurement, and its performance to generate Digital Elevation Map in real-time is assessed in a ground-based measurement test. At the same time, a first proton irradiation test is performed for the evaluation of robustness in space environment.

I. Sensor Architecture

The sensor implements at pixel level a smart triggering logic that allows rejecting the unwanted counts while identifying the laser echo (Figure 1): the pixel combines several SPAD outputs together in a stream of very short pulses (realizing what is called a digital silicon photomultiplier, or dSiPM). These pulses are then handled by a smart triggering logic, identifying the echo by finding photons which are closely spaced in time for a specified duration [2], the correlation window.

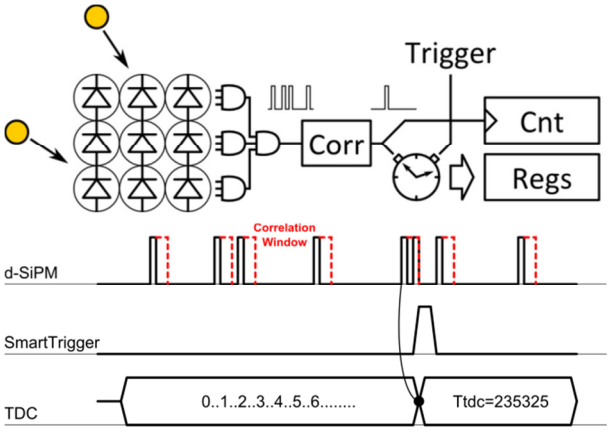

Figure 1. Principle of operation of the pixel with smart triggering

A time-to-digital converter (TDC) acts as a stopwatch, measuring the time-of-flight, while the count of photons received during the time observation window is also recorded [3].
Thanks to the smart triggering operation, the robustness to ambient light is improved and correct operation is ensured in a wide range of operating conditions, up to 100Mph/s of background light for each pixel [1].

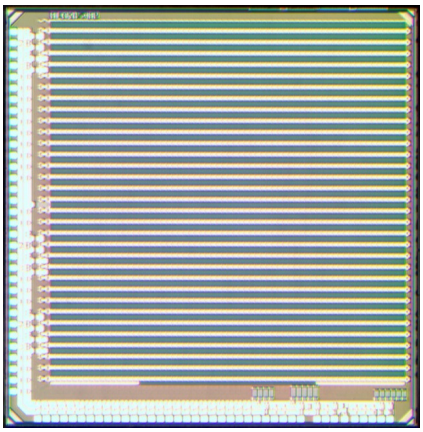

Figure 2. Chip micrograph of the 64×64-pixel sensor.

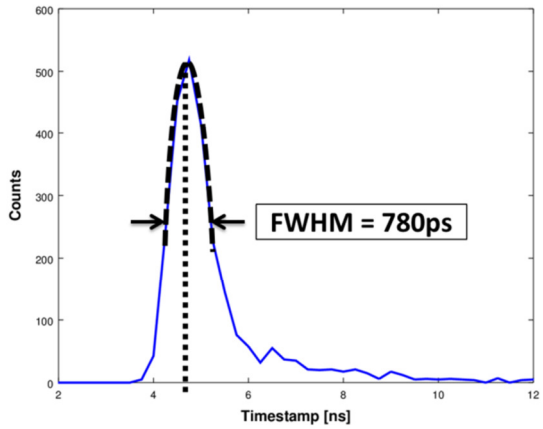

Figure 3. Timing resolution of a single pixel.

The realized sensor micrograph is depicted in Figure 2: implemented in a 150nm standard CMOS technology, it includes an array of 64×64 dSiPM-based pixels, supporting up to 17.9kfps digital readout. Each pixel contains 8 SPADs combined in a dSiPM, a smart triggering logic, a 16-bit 250-ps TDC, and a 4-bit counter. A detailed description of the architecture and circuits can be found in [1].

The histogram obtained with a 70-ps laser pulse on a single pixel is shown in Figure 3, revealing an overall 780-ps FWHM (σ_{Tph} = 331 ps) single shot timing resolution. This value, in absence of spurious counts (background or dark) means $\sigma_{z\text{-single}}$ = 5 cm single-shot TOF precision, which can be improved by statistics, i.e. building an histogram using several frames.

Indeed, the final precision can be approximated by the following expression:

$$\sigma_{z-multiple} = \frac{\sigma_{z-single}}{\sqrt{N_{frame}-(N_{BG}+N_{DCR}+N_{void})}} \qquad (1)$$

where N_{frame} is the number of points in the histogram, N_{bg} and N_{DCR} are the number of timestamps due to background and DCR, and N_{void} are the number of frames ending up without any detection. Without the use of the smart triggering logic, all background and DCR counts are reducing the useful statistics, while few frame end without any count; on the other hand, using the smart triggering, since most of the background and DCR counts are rejected, the denominator in (1) is maximized. However, the number of void frames can be increased and therefore the system parameters (laser strength, width of correlation window and laser pulse width, …) must be properly tuned.

II. Irradiation Tests

The characterized chips contained an additional test row with the possibility of selecting individual SPADs out of the dSiPM [1]. Some papers describing results of irradiation test can be found in literature but only for SPAD devices and not for complete imagers [4]. Therefore, SPADs have been characterized before and after irradiation in terms of their dark-count rate (DCR) and breakdown voltage. The irradiation has been performed using three different fluences at 50MeV proton energy, $7{\cdot}10^{10}$, $2{\cdot}10^{11}$ and $3{\cdot}10^{11}$ protons/cm^2, respectively, ranging from a low-earth orbit mission (LEO) up to a Jovian mission. After the irradiation, the three samples were operational (addressing and readout electronics correctly working) and therefore a full SPAD electrical characterization has been repeated. Figure 4 shows the DCR distribution of the three chips: as expected, the DCR increases considerably.

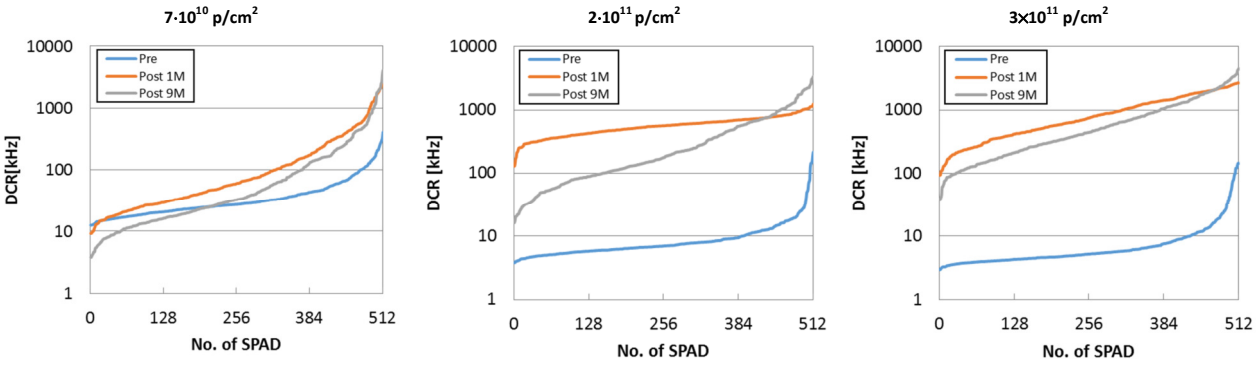

Figure 4. SPAD test row DCR distribution before irradiation, after 1 month and after 9 months, for the $7{\cdot}10^{10}$, $2{\cdot}10^{11}$ and $3{\times}10^{11}$ p/cm^2 dose, respectively (left to right).

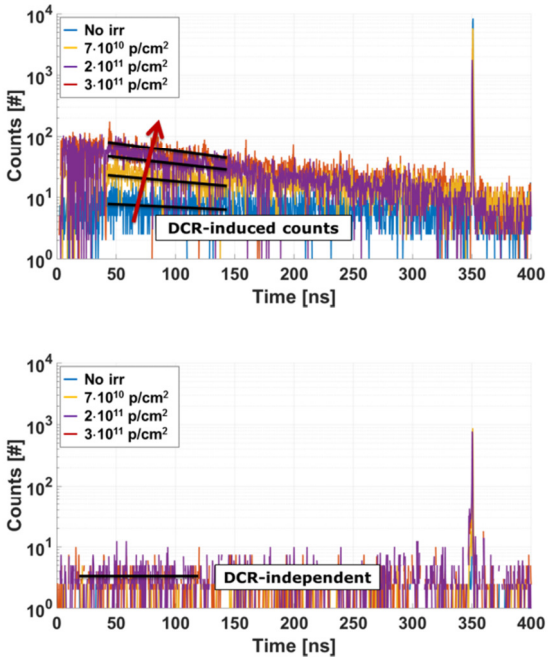

Figure 5. Count histograms obtained without and with the smart triggering enabled, for a virgin chip and for the three chips subjected to the proton irradiation.

At the same time, a small shift in the breakdown voltage towards higher values and an increase of the afterpulsing behavior has been observed. All these effects are to be attributed to the newly generated defects in the SPAD structures.

However, despite the DCR being orders of magnitude higher, the smart-triggering operation still allows correct histogram reconstruction. This can be clearly seen in Figure 5, where the histograms collected with and without the smart triggering logic are compared, for a setup condition where the laser peak is detected after a time-of-flight of 350 ns. As a reference baseline, also a non-irradiated chip has been included. With the smart trigger enabled, the number of counts due to DCR are strongly reduced, making the laser pulse easier to recognize, showing the robustness of the architecture to irradiation and therefore its suitability to the space environment.

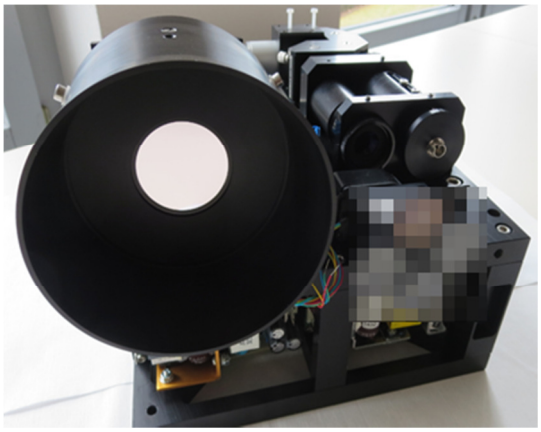

Figure 6. LiDAR system breadboard, complete with laser, sensor, optics and driving electronics.

III. LiDAR System Measurements

The DTOF image sensor has been integrated into a compact LiDAR system (25×31.4×24.4 cm^3) with a focal plane of 4 sensors of 64×64 pixels each, including proximity electronics and FPGA, optics and high-power laser module (Figure 6). Depending on the laser focusing optics, the prototype can be operated either as a single-point distance measurement device (altimeter) or as an imaging device. Due to the maximum relative velocity LiDAR-target, a 3D measurement is limited to 250 frames, obtaining a total of 128×128 per-pixel histograms of 250 pts.

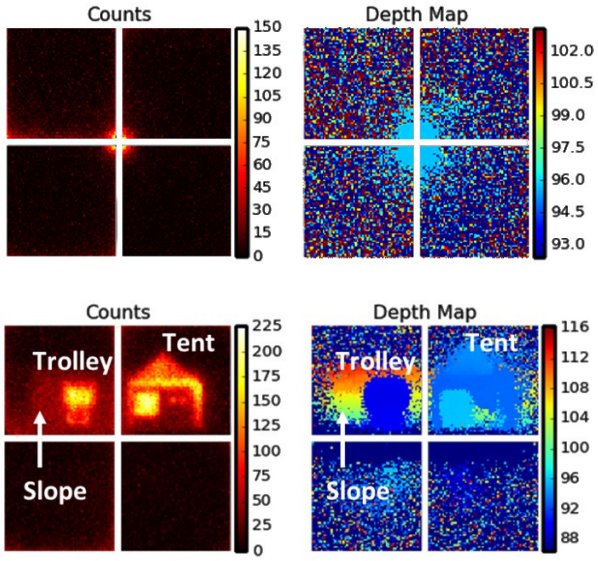

Figure 7. Long-range outdoor altimetry (top) and imaging (bottom) at 100m distance with 4 detectors in the focal plane

Several outdoor ground-based measurements have been performed, with the altimeter function and the imaging function, showing cm-range precision in both modes up to 1000m and 300m, respectively. Figure 7 shows sample images obtained during an outdoor test with 100m target distance and 250-pts histograms, achieving a precision of 3mm in altimeter mode and of 3cm in imaging mode.

In order to assess capability of generating affordable real-time digital elevation maps, the LiDAR system has been mounted on a robotic arm and dynamic tests have been performed. The results in imaging mode are shown in Figure 8, for a relative speed of 0.5 m/s, where it is possible to see that, except for a fixed offset easily removable with single-point calibration, the sensor reliably tracks the target distance. This happens without any motion-blur effect, as the acquisition and readout of the 250-pts histogram lasts only 20ms. Similar measurements have been conducted also for the altimeter mode up to 1.5m/s relative speed, confirming the correct operation.

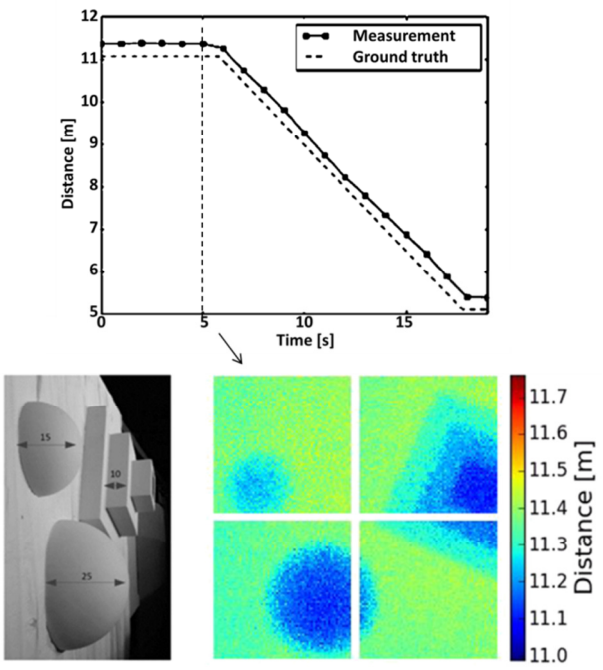

Figure 8. Dynamic tests of the LiDAR system in imaging mode: single pixel value with respect to ground truth with a speed of 0.5m/s (top), and digital elevation map recorded at t = 5s (bottom) with photograph of the target.

IV. Acknowledgments

The authors would like to thank C. Virmontois, CNES Toulouse, for the kind availability and support with the irradiation tests. The work is carried out under a programme funded by the European Space Agency (project MILA). (Disclaimer: the view expressed herein can in no way be taken to reflect the official opinion of the European Space Agency).

V. References

[1] M. Perenzoni, et al, "A 64×64-Pixel Digital Silicon Photomultiplier Direct ToF Sensor With 100Mphotons/s/pixel Background Rejection and Imaging/Altimeter Mode with 0.14% Precision up to 6km for Spacecraft Navigation and Landing", Journal of Solid-State Circuits, Jan 2017.

[2] C. Niclass, et al, "A 100-m Range 10-Frame/s 340x96-Pixel Time-of-Flight Depth Sensor in 0.18-um CMOS", Journal of Solid-State Circuits, Vol. 48, Feb. 2013.

[3] N. Dutton, et al. "A time-correlated single-photon-counting sensor with 14GS/S histogramming time-to-digital converter", International Solid-State Circuits Conference, 2015.

[4] F. Moscatelli, et al, "Radiation tests of single photon avalanche diode for space applications", Nuclear Instruments and Methods in Physics Research Section A, vol. 711, 21 May 2013, pp. 65-72.